Journal of Asian Earth Sciences 141 (2017) 259–267

Contents lists available at ScienceDirect

Journal of Asian Earth Sciences

journal homepage: www.elsevier.com/locate/jseaes

Earthquake genesis in Nepal Himalaya: A perspective from imaging of the 25th April 2015 Mw 7.8 earthquake source zone

Anand K. Pandey [a], Dipankar Saikia [b], M. Ravi Kumar [a,c,*]

[a] CSIR-National Geophysical Research Institute, Hyderabad, India
[b] Indian National Center for Ocean Information Services, Hyderabad, India
[c] Institute of Seismological Research, Gandhinagar, India

ARTICLE INFO

Article history:
Received 23 November 2015
Received in revised form 28 December 2016
Accepted 28 December 2016
Available online 31 December 2016

Keywords:
Mw 7.8 Nepal Earthquake
Receiver functions
Crustal structure
Mid-crustal ramp

ABSTRACT

The Mw 7.8 earthquake in Central Nepal nucleated in the mid-crustal ramp zone of the Main Himalayan décollement Thrust (MHT) and propagated eastward for >140 km where the largest triggered event of Mw 7.3 occurred without any surface rupture. Although it is advocated that the slip and rupture dynamics are controlled by the structural configuration of the MHT and the upper crust, precise correlation between the seismic structure and seismogenesis is hitherto scarce in the Himalaya. To address the issue, we imaged the crustal structure along three profiles covering the earthquake source region using receiver function analysis of the seismic data from the HiCLIMB and HIMNT seismic networks to understand the lateral variability. A ~5 km thick, low velocity layer is observed at the mid–crustal level, that steepens in the MHT ramp zone. The bulk of the seismicity including large shocks after the 2015 Nepal earthquake lies in the vicinity of this low velocity layer. Correlation of the seismic structure and aftershock distribution with the published crustal structure clearly suggests that the rupture involves a thicker zone extending for >40 km to the south of the source zone in the MHT ramp. We refined the structure of the MHT zone incorporating published coseismic slip and ground deformation to suggest that the rupture terminated at the footwall imbricate (horse) on the floor thrust below the zone of maximum coseismic uplift and there was a two stage rupture towards the eastern margin of the rupture zone.

1. Introduction

The 25 April 2015 earthquake of magnitude (Mw) 7.8 that occurred on a gently (7–10°) north dipping, near E–W trending thrust fault, at about 15 km depth (Fig. 1; USGS, 2015; Galetzka et al., 2015), is the largest event recorded in the Nepal Himalaya during the modern instrumental era. The rupture propagated eastward within ~40 s (Avouac et al., 2015; Yagi and Okuwaki, 2015) where most of the aftershocks were clustered and the largest aftershock/triggered earthquake of Mw 7.3 occurred on 12th May 2015 at a depth of 17 km. Over 500 local earthquakes/aftershocks with magnitude >4.0 occurred within 45 days of the main event (Fig. 1; USGS, 2015; Adhikari et al., 2015). It is construed that the hypocentre lies within the mid crustal ramp on the Main Himalayan Thrust (MHT) (Avouac et al., 2015), which is well established in this region (Ni and Barazangi, 1984; Schelling, 1992; Pearson and DeCelles, 2005; Avouac, 2015). The spatial distribution of the aftershocks defines a nearly $140 \times 40\ km^2$ rectangular fault zone that ruptured during the 2015 Nepal earthquakes (Fig. 1) abutting the presumed extension of the rupture zone of the 1934-*M* 8.4-Great Bihar Nepal earthquake (Adhikari et al., 2015). Results from InSAR line-of-sight displacement data gleaned from the ALOS-2 data show that the slip during the main shock and the largest aftershock/triggered event extends for over >140 km with a peak slip of 5.5–6.5 m on the MHT between 5 and 15 km depth and a >1 m co-seismic uplift just north of Kathmandu and a corresponding depression on either side of the uplift zone (Lindsey et al., 2015; Avouac et al., 2015; Elliott et al., 2016; Sreejith et al., 2016). The main shock and the aftershocks of the 2015-Nepal earthquake did not produce any surface rupture and the observed ground deformation (Lindsey et al., 2015; Sreejith et al., 2016; Elliott et al., 2016) largely remains confined to the Lesser Himalayan region, which constitutes the locked zone of the MHT having an interseismic strain deficit rate of around 17.8 ± 1.5 mm/yr (Ader et al., 2012; Bilham et al., 1997) for over a decade in the region. The seismogenesis in the Himalayan region is controlled by the mid–crustal ramp on the MHT, which is the source zone of the earthquakes and microseismicity (Pandey et al., 1999; Schulte-

* Corresponding author at: CSIR-National Geophysical Research Institute, Hyderabad, India.
E-mail address: mravingri@gmail.com (M.R. Kumar).

http://dx.doi.org/10.1016/j.jseaes.2016.12.039
1367-9120/

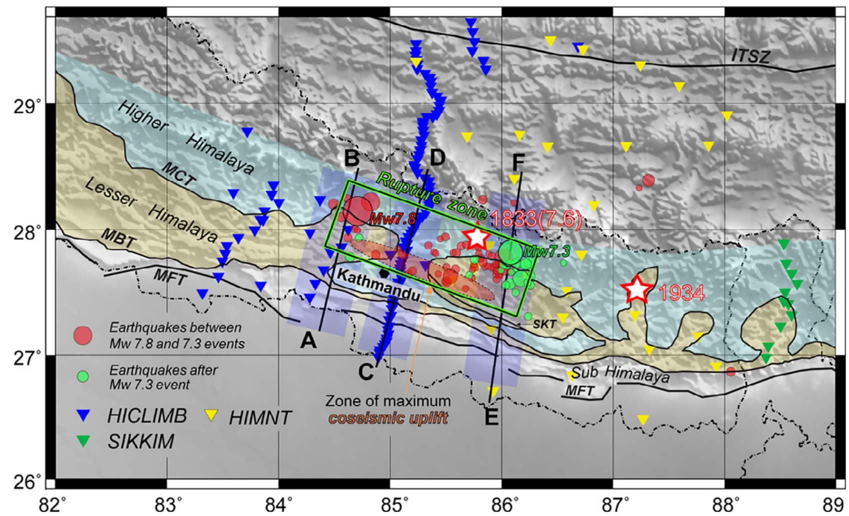

Fig. 1. Locations of the 2015 Nepal Earthquake and its aftershocks overlain on the tectonic map of the region. The rectangular box represents the rupture zone of the earthquake. AB, CD, EF are the profiles along which the receiver function images are presented. Inverted triangles are the seismic stations used in this study. Relocated epicentres of the 1934 and 1833 earthquakes are also shown.

Pelkum et al., 2005; Avouac, 2015), though its configuration is not well constrained. The large and great earthquakes rupture the southern flat of the MHT and emerge towards the Himalayan front depending on the co–seismic slip distribution and the geometry of the structures along the rupture zone (Mugnier et al., 2013; Bollinger et al., 2014; Avouac, 2015). The 25th April 2015 earthquake affected zone also experienced the Mw 7.6 – 1833 Nepal earthquake (Bilham, 1995; Mugnier et al., 2013) and the 1934-Bihar Nepal Great earthquake, which produced surface rupture and ground deformation along the MFT in the adjoining region (Sapkota et al., 2013; Bollinger et al., 2014).

In this paper, we performed common conversion point (CCP) receiver function analysis of the HiCLIMB (Nábělek et al., 2009) and HIMNT (Schulte-Pelkum et al., 2005) data along three sections AB-traversing the epicentre of the Mw 7.8 main event, CD- across Kathmandu, where maximum ground deformation is observed, and EF – across the epicentre of the largest aftershock/triggered earthquake (Fig. 1). We correlated seismic receiver function analysis results with the crustal structures along the respective sections (Pearson and DeCelles, 2005; Schelling, 1992) and integrated them with the coseismic geodetic observations (Lindsey et al., 2015) to understand the seismogenesis and rupture during the 2015 Nepal earthquake.

2. Receiver function imaging of the crust

The data accrued from the HiCLIMB and HIMNT networks offered an excellent opportunity to interrogate and validate the structure of the seismogenic zones in the Himalayan mountain belt using the receiver function (RF) analysis. Waveforms used in this study are extracted from the data base of HiCLIMB and HIMNT seismological experiments in the Nepal Himalaya and southern Tibet, archived in the IRIS Data Management Centre. However, only a subset of data from stations of the Hi-CLIMB experiment, located within our study area south of 30°N latitude is utilized (Fig. 1). Three component seismograms due to earthquakes with magnitude >5.5 in the epicentral distance range 30–90° having a P-wave SNR > 3 are selected for computation of receiver functions. A total of 1535 and 533 events that yielded good quality waveforms have a reasonably good azimuthal coverage at the HiCLIMB and HIMNT stations, respectively (Fig. 2).

Receiver function analysis is a powerful tool to investigate the receive side sub-surface structure. The receiver function method is based on the fact that the coda of the P-wave contains the P to S (Ps) conversions and their reverberations resulting from the impedance contrast across layers beneath the receiver. These Ps conversions and reverberations can be isolated through deconvolution of the vertical component from the radial component of the seismic record of a teleseismic earthquake. However, the simple concept of deconvolution is tricky to implement due to instability arising from division by zero. To avoid this instability, several methods of receiver function calculation, like the spectral water level deconvolution (Langston, 1979; Owens et al., 1983; Ammon et al., 1990), deconvolution in the time domain by least-squares estimation (Abers et al., 1995), iterative time domain deconvolution (Ligorría and Ammon, 1999) and multitaper frequency-domain cross-correlation receiver function (MTRF) (Park and Levin, 2000), have been developed. The advantage of MTRF method over the other methods is the use of multitapers to minimize spectral leakage during estimation of the spectrum and use of a pre-event noise spectrum for frequency dependent damping. A drawback of this method is that it uses a short analysis window, which limits its usability in situations where information at longer lags is desired. In this study, the receiver functions are calculated using the extended-time multitaper frequency domain technique (EMTRF) of Helffrich (2006), which is an extension of the MRTF method of Park and Levin (2000) for computing receiver functions of arbitrary length. This method uses a series of short, overlapping, multiple tapers to window the time series across its length and sums the individual Fourier transformed signals to produce a receiver function estimate which preserves the phase information for each sub-window. The vertical and horizontal components of the seismograms are decomposed into P, Sv and Sh components using the back azimuth and incidence angle estimated from the first 10 s of the seismograms around the P–wave arrival prior to applying the ETMTRF. A frequency domain low–pass $\cos^2$ taper with a cut off frequency at 1 Hz is applied to all the RFs to avoid Gibbs effect. After an initial quality check, 25,000 high quality RFs from 1848 events are retained for further processing. The common conversion point (CCP) stacking method has been used to image the structure along linear profiles shown in Fig. 1. The receiver functions are migrated to depth using Ps travel time equation and the ak135 velocity model whose crustal part is replaced by crust 1.0 (Laske